Spiral-staircase photonic structures of metallic nanorods

A. Christofi,[1,2,*] N. Stefanou,[1] G. Gantzounis,[3] and N. Papanikolaou[3]
[1]*University of Athens, Section of Solid State Physics, Panepistimioupolis, GR-157 84 Athens, Greece*
[2]*Institute of Materials Science, NCSR "Demokritos," GR-153 10 Athens, Greece*
[3]*Institute of Microelectronics, NCSR "Demokritos," GR-153 10 Athens, Greece*
(Received 25 May 2011; revised manuscript received 2 August 2011; published 8 September 2011)

By employing the layer-multiple-scattering method, properly extended to periodic assemblies of arbitrarily oriented axis-symmetric particles, we investigate the optical response of a three-dimensional spiral-staircase structure of metallic nanorods. We show that the combination of plasmonic modes and helical arrangement of the nanorods results in the formation of collective optical eigenmodes with a specific predominant circular polarization character, sizable polarization gaps, and negative group velocity bands that lead to negative refraction. Moreover, we demonstrate that multilayer slabs of the given crystal exhibit strong optical activity and circular dichroism combined with reduced dissipative losses, which make the proposed structure potentially useful for polarization control applications in miniaturized optoelectronic devices.

DOI: 10.1103/PhysRevB.84.125109 PACS number(s): 42.25.Ja, 42.70.Qs, 78.20.Ek, 78.67.Qa

I. INTRODUCTION

The fact that a chiral arrangement of the atomic/molecular constituents (structural chirality) or an inherent chiral structure of the molecules themselves (molecular chirality) is responsible for the observed optical activity in some naturally occurring substances and materials (see, e.g., Ref. 1 and references therein) has long motivated microwave studies on model systems of macroscopic bodies with helical symmetry.[2–5]

More recently, in the context of photonic crystals,[6] three-dimensional (3D) chiral dielectric structures were first proposed as artificial composite media that exhibit strong optical activity.[7,8] Subsequently, such structures were found to possess sizable omnidirectional photonic band gaps,[9,10] as well as partial band gaps for just one of the two circular polarizations[11,12] that can give rise to strong circular dichroism.[13–15] On the other hand, it has been shown that chiral architectures of metallic building units can exhibit a huge optical activity, which exceeds by several orders of magnitude that of natural chiral materials,[16–26] thus opening new perspectives in the design of subwavelength optical components for polarization control applications.[27]

In recent years, these chiral metallodielectric architectures attract growing interest also in relation to negative-index metamaterials.[28–43] In most of these studies, artificial gyrotropic structures are realized as one or two layers of chiral resonators, and their exotic properties are interpreted by a numerical approach assuming applicability of effective medium theory and retrieving effective constitutive parameters from transmission and reflection spectra at normal incidence. However, these structures are strongly anisotropic and their optical response cannot be always described by means of local effective material parameters.[44] Moreover, even assigning effective wave parameters, such as a scalar refractive index that refers to a specific mode and a particular direction of propagation, may be problematic, especially in the strong-coupling regime.[45] In any case, the refractive properties of the medium cannot be deduced from the refractive index and, therefore, a direct demonstration of negative refraction in such chiral metamaterials is necessary.

In this paper, we report a thorough investigation of the optical properties of a 3D spiral-staircase structure of metallic nanorods by means of rigorous full-electrodynamic calculations. We analyze the nature of the photonic eigenmodes of this crystal in the light of group theory and explain their physical origin. Moreover, we study the change in the polarization state of a wave transmitted through a finite slab of the crystal and reveal the occurrence of strong optical activity effects. Finally, we provide a consistent interpretation of negative refraction, which can occur within certain regions of frequency and angles of incidence on a specific surface of the crystal, by reference to relevant isofrequency contours obtained from detailed photonic band-structure calculations. It is worth noting that the structure under consideration does not support purely left- and right-circularly polarized (LCP and RCP, respectively) eigenmodes, in contrast to mostly studied chiral metamaterials with, e.g., C_4 symmetry.[17–23,34–36,38–40,42,43,45,46] In this respect, our results and analysis apply to a broader class of chiral structures of lower symmetry, made of resonant plasmonic components in helical arrangement, and explain aspects of their optical response to a degree that goes beyond existing interpretation. On the other hand, our theoretical method is ideally suited for the study of such multilayered chiral metamaterials, combining computational efficiency with physical clarity.

II. METHOD OF CALCULATION

Our calculations are carried out using the full-electrodynamic layer-multiple-scattering (LMS) method,[47–49] which is ideally suited for stratified structures consisting of successive layers of nonoverlapping particles (scatterers) of arbitrary shape, arranged with the same two-dimensional (2D) periodicity in the x-y plane, while periodicity in the z direction is not a prerequisite. In the spirit of the multiple-scattering approach, the scattering properties of the whole composite structure are obtained from those of the individual building units. The main idea of the LMS method relies on the combined optimal use of two distinct basis sets. (a) A spherical-wave basis for the description of in-plane multiple scattering, which

insures fast convergence for scatterers of not too large size parameter and not too strong deviation from the spherical shape. (b) A plane-wave basis for the description of interlayer multiple scattering, which takes advantage of the common 2D periodicity of the different layers. The method solves Maxwell equations in frequency domain and thus dispersion and absorptive losses in the constituent materials can be readily included. Besides the complex photonic band structure of an infinite crystal, associated with a given crystallographic plane, the LMS method can also provide the reflectance, transmittance, and absorbance of a finite slab of the crystal at any angle of incidence and, in this respect, it can describe an actual transmission experiment.

The properties of the individual scatterers enter through the corresponding scattering T matrix in a spherical-wave representation Plm; $P = 1,2$ denotes magnetic and electric multipoles, respectively, while $l = 1,2,\ldots$ and $m = -l, -l+1,\ldots,l$ are the usual angular momentum indices. For particles of cylindrical symmetry, in a coordinate system defined by taking the z axis along the axis of revolution of the particle, the elements of the T matrix, $T^0_{Plm;P'l'm'}$, are identically zero if $P+l+m$ and $P'+l'+m'$ do not have the same parity.[49] This symmetry property, however, does not hold in any coordinate system. If α,β,γ are the Euler angles transforming an arbitrarily chosen coordinate system into the particle coordinate system, the T matrix is given by

$$T_{Plm;P'l'm'} = \sum_{m_1=-l}^{l}\sum_{m'_1=-l'}^{l'} D^{(l)}_{mm_1}(\alpha,\beta,\gamma)T^0_{Plm_1;P'l'm'_1} \times D^{(l')}_{m'_1m'}(-\gamma,-\beta,-\alpha), \quad (1)$$

where T^0 refers to the particle coordinate system and $D^{(l)}$ are the appropriate transformation matrices associated with the l irreducible representation of the $O(3)$ group.[50] Therefore, starting from T^0, which is calculated efficiently by the extended-boundary-condition method,[51] we can obtain the T matrix in a rotated coordinate system through Eq. (1).

Within the LMS method,[49] at a first step, in-plane multiple scattering is evaluated in the specific spherical-wave basis using the T matrix of the individual scatterers and appropriate propagator functions. Subsequently, interlayer coupling is fully taken into account by properly combining the transmission and reflection matrices of the component layers, such as the x-y layers of Fig. 1, so as to describe multiple scattering between the layers to any order, in a plane-wave representation defined as follows. We write the component of the wave vector of the incident plane wave parallel to the layers, $\mathbf{q}_\parallel$, as $\mathbf{q}_\parallel = \mathbf{k}_\parallel + \mathbf{g}'$, where $\mathbf{k}_\parallel$, the reduced wave vector in the surface Brillouin zone, is a conserved quantity in the scattering process and $\mathbf{g}'$ is a certain reciprocal vector of the given 2D lattice. Therefore, the wave vector of the incident wave has the form $\mathbf{K}^{\pm}_{\mathbf{g}'} = \mathbf{k}_\parallel + \mathbf{g}' \pm [q^2 - (\mathbf{k}_\parallel + \mathbf{g}')^2]^{1/2}\hat{\mathbf{e}}_z$, where q is the wave number, $\hat{\mathbf{e}}_z$ is the unit vector along the z axis, and the $+$ or $-$ sign refers to incidence from $z<0$ or from $z>0$, i.e., a wave propagating toward the positive or negative z direction, respectively. Since $\mathbf{k}_\parallel$ and the angular frequency ω are conserved quantities, the scattered field will consist of a series of plane waves with wave vectors

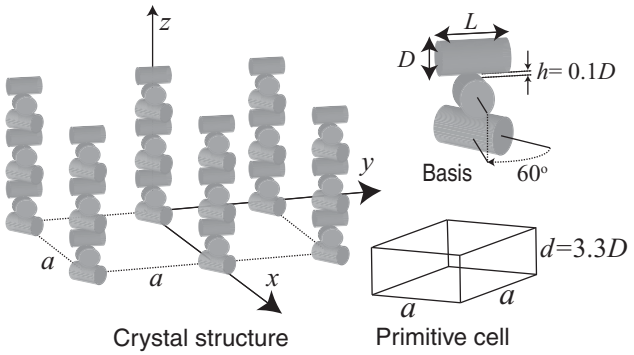

FIG. 1. Spiral-staircase structure of metallic nanorods under consideration.

$$\mathbf{K}^{\pm}_{\mathbf{g}} = \mathbf{k}_\parallel + \mathbf{g} \pm [q^2 - (\mathbf{k}_\parallel + \mathbf{g})^2]^{1/2}\hat{\mathbf{e}}_z, \quad \forall \mathbf{g}, \quad (2)$$

and polarizations along $\hat{\mathbf{e}}_1$ and $\hat{\mathbf{e}}_2$ (polar and azimuthal unit vectors, respectively, associated with every $\mathbf{K}^s_{\mathbf{g}}$, $s = \pm$). It is worth noting that, though the scattered field consists, in general, of a number of diffracted beams corresponding to different 2D reciprocal lattice vectors $\mathbf{g}$, only beams for which $\mathbf{K}^s_{\mathbf{g}z}$ is real constitute propagating waves. When $(\mathbf{k}_\parallel + \mathbf{g})^2 > q^2$, we have an evanescent beam and the corresponding unit vectors $\hat{\mathbf{e}}_1,\hat{\mathbf{e}}_2$ become complex, but they are still orthonormal: $\hat{\mathbf{e}}_p \cdot \hat{\mathbf{e}}_{p'} = \delta_{pp'}$, $p(p') = 1,2$.

The ratio of the transmitted or reflected energy flux to the energy flux associated with the incident wave defines the transmittance, $\mathcal{T}$, or reflectance, $\mathcal{R}$, respectively, of a multilayer slab. On the other hand, for a 3D crystal consisting of an infinite periodic sequence of layers, stacked along the z direction, applying the Bloch condition for the wave field in the region between two consecutive unit slabs leads to an eigenvalue equation, which gives the z component of the Bloch wave vector, k_z, for the given ω and $\mathbf{k}_\parallel$. The eigenvalues $k_z(\omega,\mathbf{k}_\parallel)$, looked upon as functions of real ω, define, for each $\mathbf{k}_\parallel$, lines in the complex k_z plane. Taken together they constitute the complex band structure of the infinite crystal associated with the given crystallographic plane. A line of given $\mathbf{k}_\parallel$ may be real (in the sense that k_z is real) over certain frequency regions, and be complex (in the sense that k_z is complex) for ω outside these regions. It turns out that, for given $\mathbf{k}_\parallel$ and ω, out of the eigenvalues $k_z(\omega,\mathbf{k}_\parallel)$, none or, at best, a few are real and the corresponding eigenvectors represent propagating modes of the electromagnetic (EM) field in the given infinite crystal. The remaining eigenvalues $k_z(\omega,\mathbf{k}_\parallel)$ are complex and the corresponding eigenvectors represent evanescent waves. These have an amplitude that increases exponentially in the positive or negative z direction and, unlike the propagating waves, do not exist as physical entities in the infinite crystal. However, they are an essential part of the physical solutions of the EM field in a slab of finite thickness. A region of frequency where propagating waves do not exist, for given $\mathbf{k}_\parallel$, constitutes a frequency gap of the EM field for the given $\mathbf{k}_\parallel$. If, over a frequency region, no propagating wave exists whatever the

value of $\mathbf{k}_\parallel$, then this region constitutes an absolute frequency gap.

III. RESULTS AND DISCUSSION

A. Photonic band structure

We consider a layer-by-layer structure of metallic nanorods of length L, with a circular cross section of diameter D, stacked along the z direction. In each layer, the nanorods are centered at the sites of a square lattice, of lattice constant a, with their axes aligned in a direction perpendicular to the z axis. The nanorods in consecutive layers are mutually twisted through an angle of 60° and are separated by a distance h, equal to one-tenth of their diameter, as shown in Fig. 1. Therefore, the period d of the structure along the z direction comprises three layers ($d = 3.3D$). With this particular choice of parameters, we obtain strong effects with reduced computational effort, though other choices for the twisting angle and interlayer spacing lead to similar results. Obviously, the crystal under consideration lacks invariance under space inversion because of the helical arrangement of the nanorods and thus the appropriate point symmetry group is D_2, which consists of only proper rotations, and not D_{2h} that would be if all nanorods were aligned.[50]

We assume, to begin with, that the metallic material is described by the Drude dielectric function,[52]

$$\epsilon_m(\omega) = 1 - \frac{\omega_p^2}{\omega(\omega + i\tau^{-1})}, \tag{3}$$

where ω_p is the bulk plasma frequency and τ the relaxation time of the conduction band electrons, and we take $D = c/\omega_p$, $L = 2.5c/\omega_p$, and $a = 7.5c/\omega_p$. We note that, assuming $\hbar\omega_p \cong 10$ eV, the diameter of the nanorods, D, corresponds to about 20 nm and their length, L, to about 50 nm.

In order to ensure adequate convergence of our calculations for the given structure, we truncate the spherical-wave expansions at $l_{\max} = 8$ and take into account 69 2D reciprocal lattice vectors $\mathbf{g}$ in the relevant plane-wave expansions, while the single-particle scattering T matrix is evaluated with $l_{\text{cut}} = 15$ and a Gaussian quadrature integration formula with 1024 points.[49]

In Fig. 2, we display the photonic band structure of the given crystal along its [001] direction, calculated by deliberately disregarding absorptive losses taking $\tau^{-1} = 0$ in Eq. (3) in order to ensure an unambiguous interpretation of the dispersion diagram. The bands along this direction are nondegenerate and have the symmetry of the irreducible representations (A, B) of the C_2 group, which is a subgroup of D_2,[50] i.e., the corresponding eigenmodes are even (A) or odd (B) upon rotation through 180° about the z axis. Only the symmetry of the B bands is appropriate for an EM wave incident normally on the (001) surface of the crystal, thus allowing for light transmission. The A bands (such bands do not exist in the frequency region under consideration, but appear at higher frequencies) cannot be excited by an externally incident EM wave because they do not have the proper symmetry; they correspond to bound states of the EM field in a finite (001) slab of the crystal, which decrease exponentially outside the slab on either side of it. It is worth noting that the C_2 symmetry does not allow for the existence of LCP and RCP eigenmodes,

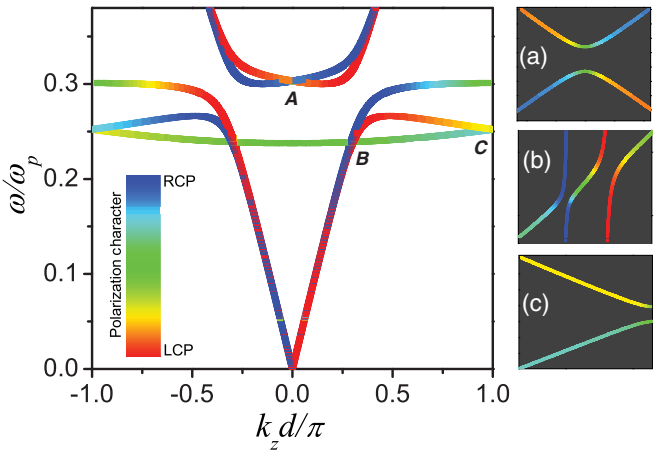

FIG. 2. (Color online) Photonic band structure of the crystal of Fig. 1 along its [001] direction. The optical response of the metallic nanorods is described by the Drude dielectric function of Eq. (3) without dissipative losses ($\tau^{-1} = 0$) and the geometric parameters of the structure are $D = c/\omega_p$, $L = 2.5c/\omega_p$, and $a = 7.5c/\omega_p$. An enlarged view of the dispersion diagram about the crossing points (A, B, C) is shown in the margin.

as would be the case under, e.g., the fourfold rotation (C_4) symmetry.[50] In our case, each optically active B band has a different degree of LCP and RCP admixture that varies along the band as shown in Fig. 2. However, since all bands in the dispersion diagram of Fig. 2 have the same symmetry (B) in terms of group theory, anticrossing interaction between them always takes place and removes degeneracies to a major or minor degree depending on the shape of the modes involved.

A careful analysis of the dispersion diagram of Fig. 2 reveals the existence of (a) two extended bands, one of LCP and one of RCP predominant character, associated with wave propagation in an underlying effective medium and (b) three narrow bands, i.e., as many as the number of nanorods per primitive cell, originating from the fundamental longitudinal dipole-like plasmon modes of the individual nanorods at $0.30\omega_p$,[53] weakly interacting between them. The lowest of these narrow bands, about $0.25\omega_p$, has a mixed LCP-RCP character and interacts weakly with the other bands, giving rise to very small hybridization gaps about the crossing points, which are hardly discernible [see insets (b) and (c) in Fig. 2]. The other two narrow bands, one of LCP and one of RCP predominant character extending from $0.25\omega_p$ to $0.30\omega_p$, interact strongly with the corresponding effective-medium bands leading to the occurrence of considerable hybridization gaps for a specific polarization. The (weak) anticrossing interaction between these two narrow bands at the Brillouin zone center reverses the predominant polarization character of the resulting dispersion curves about $k_z = 0$ in an abrupt but continuous manner, as shown in the corresponding inset (a) to Fig. 2. The photonic band structure of the crystal under consideration is very similar to that of the metallic helix arrays studied by Wu *et al.*[41] Therefore, our rigorous group-theory analysis is applicable to a wide class of chiral metamaterials and explains salient features of their dispersion diagrams to a degree that goes beyond existing interpretation.

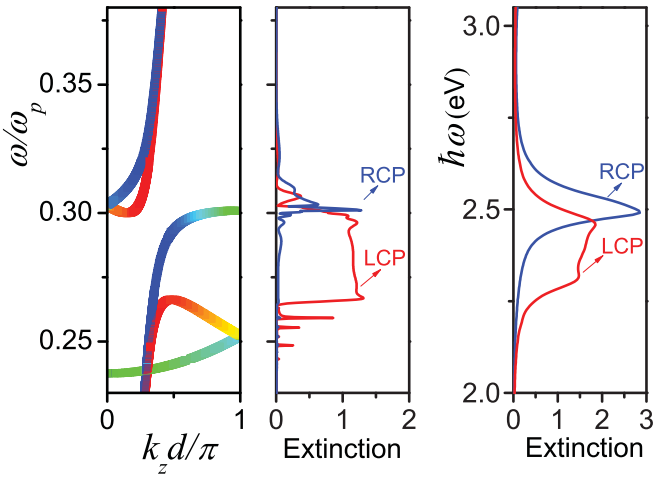

FIG. 3. (Color online) Photonic band structure of Fig. 2 for positive values of k_z (left-hand diagram) and the extinction of LCP and RCP light incident along the positive z direction on a (001) slab of the crystal consisting of 24 layers of nanorods (middle diagram). The corresponding extinction spectra if the slab is made of silver nanorods described by the experimental dielectric function of bulk silver[54] and the geometric parameters of the structure are $D = 20$ nm, $L = 50$ nm, and $a = 150$ nm are displayed in the right-hand diagram.

The above eigenmode analysis is consistent with corresponding extinction spectra of finite slabs of the given crystal. The extinction is defined, as usual, as $-\ln \mathcal{T}$, with $\mathcal{T}$ being the transmittance of the slab. Modes with a certain predominant circular-polarization character and positive (negative) group velocity couple predominantly to a plane EM wave with the same polarization, incident along the positive (negative) z direction on a (001) slab of the crystal. As shown in Fig. 3, over the frequency range of a polarization gap, only incident waves of opposite handedness are allowed to pass through. Such regions of polarization-selective transmission have also been observed in metallic helix arrays.[26,41]

B. Optical activity

The polarization state of a wave transmitted through a finite slab of the crystal under consideration is directly obtained from the corresponding transmission matrix. It is worth noting that, in the frequency region under consideration, we are below the diffraction limit for light incident normally on the (001) surface of the crystal: $\omega/c < g_{\min} = 2\pi/a$. Therefore, only the zero-order diffraction channel yields a propagating beam and the (electric-field) amplitude of the transmitted wave is obtained from that of the incident wave through a 2×2 complex transmission matrix, $\mathbf{t}$, as follows:

$$E_p^{\rm tr} = \sum_{p'} t_{pp'} E_{p'}^{\rm in}, \tag{4}$$

where $p(p') = 1,2$ refers to the linearly polarized waves with the electric field oscillating in or perpendicular to the plane of incidence, respectively, in accordance with the plane-wave basis employed in the LMS method (see Sec. II). We note that, at normal incidence on the (001) surface of the crystal, these polarization directions coincide with the x and y axes, respectively. In the basis of circular-polarization states, the transmission matrix takes the form

$$\mathbf{t} = \begin{pmatrix} t_{LL} & t_{LR} \\ t_{RL} & t_{RR} \end{pmatrix} = \tfrac{1}{2}\begin{pmatrix} t_{11}+t_{22}+i(t_{21}-t_{12}) & t_{11}-t_{22}+i(t_{21}+t_{12}) \\ t_{11}-t_{22}-i(t_{21}+t_{12}) & t_{11}+t_{22}-i(t_{21}-t_{12}) \end{pmatrix}, \tag{5}$$

where $p(p') = L, R$ denotes LCP and RCP states, respectively. An incoming plane wave of amplitude E_0, propagating along the positive z direction, linearly polarized at an angle ϕ_0 with respect to the x axis, can be decomposed into LCP and RCP waves of amplitudes $E_L^{\rm in} = E_0 \exp(-i\phi_0)/\sqrt{2}$ and $E_R^{\rm in} = E_0 \exp(i\phi_0)/\sqrt{2}$, respectively. The corresponding transmitted fields have amplitudes

$$E_L^{\rm tr} = \frac{E_0}{\sqrt{2}}[t_{LL}\exp(-i\phi_0) + t_{LR}\exp(i\phi_0)], \tag{6}$$

$$E_R^{\rm tr} = \frac{E_0}{\sqrt{2}}[t_{RL}\exp(-i\phi_0) + t_{RR}\exp(i\phi_0)], \tag{7}$$

which correspond to an, in general, elliptically polarized wave with the long axis of the ellipse forming an angle

$$\phi = \frac{1}{2}\left[\arg\left(E_R^{\rm tr}\right) - \arg\left(E_L^{\rm tr}\right)\right] \tag{8}$$

with the x axis and with ellipticity angle

$$\chi = \arctan\frac{\left|E_R^{\rm tr}\right| - \left|E_L^{\rm tr}\right|}{\left|E_R^{\rm tr}\right| + \left|E_L^{\rm tr}\right|}, \tag{9}$$

as shown in Fig. 4. We adopt the polarization azimuth rotation angle, $\Delta\phi = \phi - \phi_0$, as a measure of circular birefringence and the ellipticity angle χ as a measure of circular dichroism. It is worth noting that, under the C_2 symmetry, circular polarization conversion takes place through the nondiagonal elements t_{LR} and t_{RL} that do not vanish identically. Therefore,

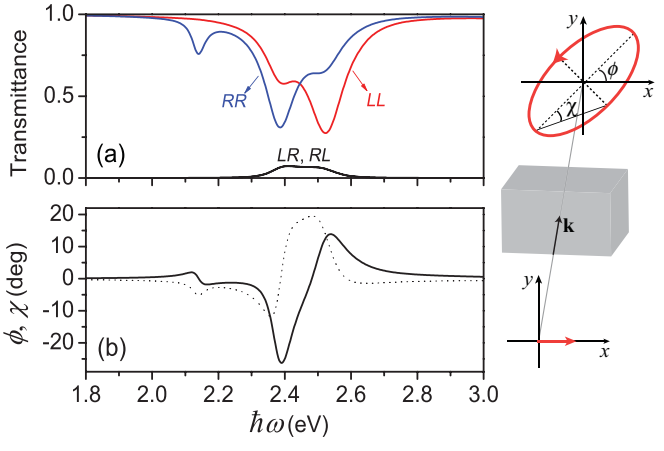

FIG. 4. (Color online) (a) Transmission spectra associated with different circular polarization channels at normal incidence on a (001) unit slab of the crystal of Fig. 1 consisting of three layers of silver nanorods ($D = 20$ nm, $L = 50$ nm, and $a = 150$ nm). (b) Corresponding polarization azimuth rotation (solid line) and ellipticity (dotted line) angles of the transmitted wave for incident wave linearly polarized along the x axis, as shown in the margin, vs frequency.

$\Delta\phi$ and χ depend on the polarization angle of the incident wave, ϕ_0.

Figure 4(a) shows the transmission properties of a (001) unit slab of the crystal of Fig. 1 consisting of three layers of silver nanorods with geometric parameters $D = 20$ nm, $L = 50$ nm, and $a = 150$ nm, at normal incidence. For the dielectric function of silver, we interpolated to the bulk values measured by Johnson and Christy[54] that include dissipative losses. It can be seen that the transmission spectra associated with the LCP and RCP channels exhibit pronounced differences, while the occurrence of cross-coupling transmission from LCP to RCP and vice versa implies a non-negligible circular polarization conversion. Therefore, circular birefringence and dichroism cannot be deduced solely from the LL and RR transmission channels and both properties vary in an oscillatory manner with the polarization angle of the incident wave. In Fig. 4(b), we depict the calculated polarization azimuth rotation and ellipticity angles of the transmitted wave for an incident wave linearly polarized along the x axis, in the spectral region of interest. At 2.38 eV the ellipticity angle vanishes, which indicates a pure optical activity effect. At this frequency, for the given linearly polarized incident wave, the transmitted wave is also linearly polarized with its plane of polarization forming an angle $\phi = -26^\circ$ with the x axis. In terms of rotatory power per sample thickness equal to one wavelength, the optical activity of the considered three-layers slab, $\phi/\lambda = -205^\circ$, is many orders of magnitude larger than that of naturally occurring optically active materials and comparable with that of other chiral metamaterials.[34] Stronger optical activity effects are obtained for thicker slabs (see Supplemental Material[55]), while the spectral response can be tuned in a controllable manner by choosing the rod length so as to appropriately shift its plasmon resonance.[53] Moreover, transmission losses are quite low, typically a few dB. This can be inferred from the right-hand diagram of Fig. 3, where transmission losses even in gap regions and for relatively thick slabs do not exceed ~ 10 dB. Therefore, multilayer slabs of the given crystal may be useful for practical applications as ultrathin circular polarizers and polarization rotators.

C. Isofrequency contours and negative refraction

The proposal that negative refraction and related effects could be easier to achieve in chiral media for one circular polarization[28–30] fueled extensive research on the design of artificial gyrotropic structures. In most of the recent studies, the negative refractive behavior of these structures was deduced by retrieving effective constitutive parameters from the transmission and reflection spectra at normal incidence on a finite slab of the metamaterial, one or two layers thick.[34–40,42,43] However, also because such chiral structures are strongly anisotropic, a direct demonstration of negative refraction of light incident at a specific angle on a given surface of the semi-infinite metamaterial is highly desirable.[41] Here, we provide evidence for the occurrence of negative refraction in the chiral crystal under consideration by examining the direction of the relevant group velocities, obtained from the exact form of the calculated isofrequency surfaces. The optical response of the metallic nanorods is described by the Drude dielectric function of Eq. (3) without dissipative losses

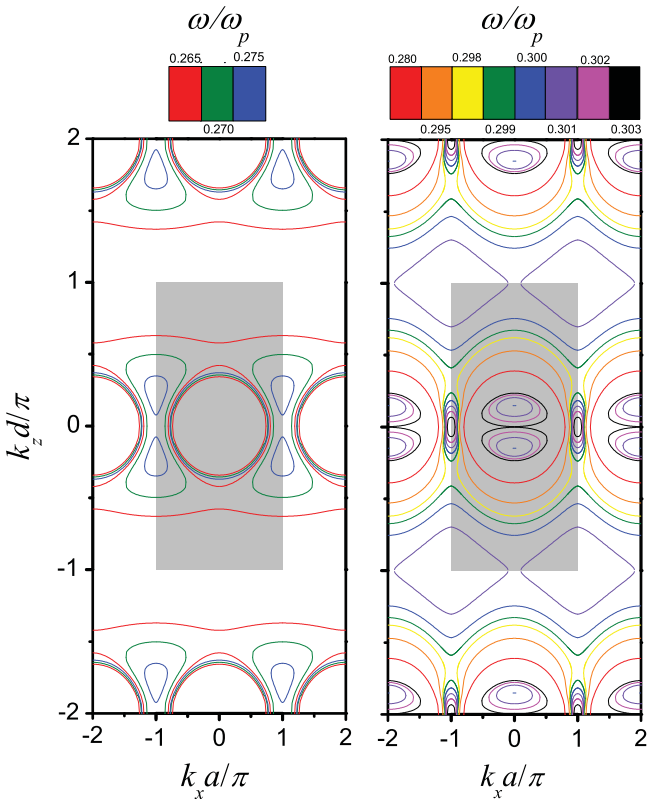

FIG. 5. (Color online) Isofrequency contours in the k_x-k_z plane ($k_y = 0$) for the crystal of Fig. 1. The optical response of the metallic nanorods is described by the Drude dielectric function of Eq. (3) without dissipative losses ($\tau^{-1} = 0$) and the geometric parameters of the structure are $D = c/\omega_p$, $L = 2.5c/\omega_p$, and $a = 7.5c/\omega_p$. The shaded rectangle shows the projection of the Brillouin zone on this plane.

($\tau^{-1} = 0$) and the geometric parameters of the structure are $D = c/\omega_p$, $L = 2.5c/\omega_p$, and $a = 7.5c/\omega_p$.

Figure 5 displays isofrequency contours, $\omega(\mathbf{k}) = \text{const}$, in the k_x-k_z plane ($k_y = 0$), in the frequency region of interest, which are appropriate for the description of the refractive properties of the crystal when the plane of incidence is the x-z plane. This corresponds to the cases of incidence on the x-y and on the y-z crystallographic surfaces, with $k_y = 0$. If a plane EM wave of angular frequency ω impinges on the x-y surface of the crystal with $\mathbf{q}_\parallel = \mathbf{k}_\parallel = (k_x,0)$, the wave-vector component parallel to the surface, k_x, is conserved and thus the points of the corresponding isofrequency curve with the same specific value of their k_x coordinate provide all possible wave vectors for the transmitted waves. The actual transmitted waves are determined from the proper direction of the corresponding group velocity, $\mathbf{v} = \nabla_{\mathbf{k}}\omega(\mathbf{k})$, which must be pointing inside the crystal. For example, if the crystal occupies the $z > 0$ half-space, v_z must be positive. A careful inspection of Fig. 5 indicates that, for any value of ω and k_z within the given frequency region, the group velocities of the transmitted waves are such that $v_x k_x > 0$, i.e., we always have regular (positive) refraction. On the contrary, if we consider incidence on the y-z surface of the crystal with $\mathbf{q}_\parallel = \mathbf{k}_\parallel = (0,k_z)$, the conserved wave-vector component parallel to the surface is k_z and then we can have $v_z k_z < 0$, i.e., negative refraction, as

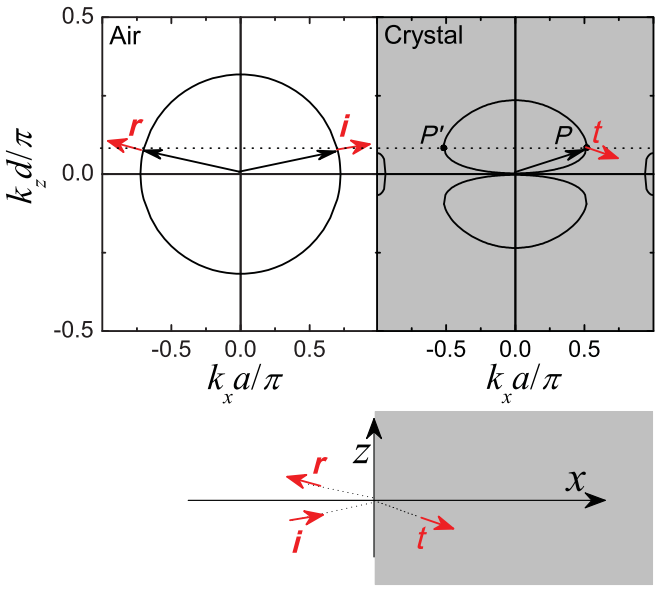

FIG. 6. (Color online) Isofrequency-contour analysis of the refraction of light of angular frequency $\omega = 0.303\omega_p$ incident from air on the y-z surface of the crystal of Fig. 1 with $\mathbf{k}_\parallel = (0, k_z)$. The optical response of the metallic nanorods is described by the Drude dielectric function of Eq. (3) without dissipative losses ($\tau^{-1} = 0$) and the geometric parameters of the structure are $D = c/\omega_p$, $L = 2.5c/\omega_p$, and $a = 7.5c/\omega_p$. The wave vectors and the group velocities of the incident (i), reflected (r), and transmitted (t) waves are indicated by long and short arrows, respectively. The dotted horizontal line in the upper diagrams is the k_z-conservation line. The lower diagram shows negative refraction in real space, in the case considered.

shown in Fig. 6 for light of angular frequency $\omega = 0.303\omega_p$ incident from air. In this case, we obtain negative refraction for $k_z d/\pi < 0.1$, i.e., for angles of incidence less than $\sim 9^\circ$. Considering $k_z d/\pi = 0.07$, the k_z-conservation line crosses the proper isofrequency contour of the crystal at two points, P and P'. The Bloch wave defined at point P' is backward propagating with respect to the interface and thus it is not a physically acceptable transmitted wave. Therefore, we obtain a single negatively refracted beam from point P, as shown in Fig. 6. Its origin traces to the negative slope of the dispersion curve about point A in Fig. 2 ($v_z k_z < 0$), which also persists for other values of k_x besides $k_x = 0$. It is worth noting that, at smaller angles of incidence, the k_z-conservation line also crosses the second branches of the specific isofrequency contour in the crystal (at larger values of k_x) and thus a second negatively refracted beam is excited (see Fig. 6).

IV. CONCLUSIONS

In summary, we reported a comprehensive study of the optical properties of a 3D helical structure of metallic nanorods by means of rigorous full-electrodynamic calculations using the LMS method, properly extended to describe axis-symmetric scatterers with arbitrary orientation. We analyzed the photonic band structure of the crystal in conjunction with relevant polarization-resolved transmission spectra and explained the nature of the different eigenmodes in the light of group theory to a degree that goes beyond existing interpretation. We demonstrated the occurrence of negative refraction in certain frequency regions and angles of incidence on a specific crystallographic surface by reference to relevant isofrequency contours and showed that multilayer slabs of the crystal exhibit strong optical activity and circular dichroism with relatively low dissipative losses.

ACKNOWLEDGMENT

A.C. was financially supported by NCSR "Demokritos."

*aristi@ims.demokritos.gr

[1] S. F. Mason, *Molecular Optical Activity and the Chiral Discriminations* (Cambridge University Press, Cambridge, UK, 1982).
[2] J. C. Bose, Proc. R. Soc. London **63**, 146 (1898).
[3] K. F. Lindman, Ann. Phys. (Leipzig) **368**, 621 (1920); **374**, 270 (1922).
[4] I. Tinoco, Jr. and M. P. Freeman, J. Phys. Chem. **61**, 1196 (1957).
[5] D. L. Jaggard and N. Engheta, Electron. Lett. **25**, 173 (1989).
[6] J. D. Joannopoulos, S. G. Johnson, J. N. Winn, and R. D. Meade, *Photonic Crystals: Molding the Flow of Light*, 2nd ed. (Princeton University Press, Princeton, NJ, 2008).
[7] V. Karathanos, N. Stefanou, and A. Modinos, J. Mod. Opt. **42**, 619 (1995).
[8] I. Hodgkinson, Q. H. Wu, B. Knight, A. Lakhtakia, and K. Robbie, Appl. Opt. **39**, 642 (2000).
[9] A. Chutinan and S. Noda, Phys. Rev. B **57**, R2006 (1998).
[10] O. Toader and S. John, Science **292**, 1133 (2001).
[11] J. Lee and C. Chan, Opt. Express **13**, 8083 (2005).
[12] M. Thiel, M. Decker, M. Deubel, M. Wegener, S. Linden, and G. von Freymann, Adv. Mater. **19**, 207 (2007).
[13] P. C. P. Hrudey, B. Szeto, and M. J. Brett, Appl. Phys. Lett. **88**, 251106 (2006).
[14] S. Furumi and Y. Sakka, Adv. Mater. **18**, 775 (2006).
[15] M. Mitov and N. Dessaud, Nat. Mater. **5**, 361 (2006).
[16] Y. Svirko, N. Zheludev, and M. Osipov, Appl. Phys. Lett. **78**, 498 (2001).
[17] A. Papakostas, A. Potts, D. M. Bagnall, S. L. Prosvirnin, H. J. Coles, and N. I. Zheludev, Phys. Rev. Lett. **90**, 107404 (2003).
[18] T. Vallius, K. Jefimovs, J. Turunen, P. Vahimaa, and Y. Svirko, Appl. Phys. Lett. **83**, 234 (2003).
[19] M. Kuwata-Gonokami, N. Saito, Y. Ino, M. Kauranen, K. Jefimovs, T. Vallius, J. Turunen, and Y. Svirko, Phys. Rev. Lett. **95**, 227401 (2005).
[20] A. V. Rogacheva, V. A. Fedotov, A. S. Schwanecke, and N. I. Zheludev, Phys. Rev. Lett. **97**, 177401 (2006).
[21] E. Plum, V. A. Fedotov, A. S. Schwanecke, N. I. Zheludev, and Y. Chen, Appl. Phys. Lett. **90**, 223113 (2007).
[22] B. Bai, Y. Svirko, J. Turunen, and T. Vallius, Phys. Rev. A **76**, 023811 (2007).
[23] D. H. Kwon, P. L. Werner, and D. H. Werner, Opt. Express **16**, 11802 (2008).
[24] C. Rockstuhl, C. Menzel, T. Paul, and F. Lederer, Phys. Rev. B **79**, 035321 (2009).

[25] A. Demetriadou and J. B. Pendry, J. Phys. Condens. Matter **21**, 376003 (2009).
[26] J. K. Gansel, M. Thiel, M. S. Rill, M. Decker, K. Bade, V. Saile, G. von Freymann, S. Linden, and M. Wegener, Science **325**, 1513 (2009).
[27] G. Shvets, Appl. Phys. Lett. **89**, 141127 (2006).
[28] S. Tretyakov, I. Nefedof, A. Sihvola, S. Maslovski, and C. Simovski, J. Electromagn. Waves Appl. **17**, 695 (2003).
[29] J. B. Pendry, Science **306**, 1353 (2004).
[30] C. Monzon and D. W. Forester, Phys. Rev. Lett. **95**, 123904 (2005).
[31] Y. Jin and S. He, Opt. Express **13**, 4974 (2005).
[32] Q. Cheng and T. J. Cui, Phys. Rev. B **73**, 113104 (2006).
[33] V. Yannopapas, J. Phys. Condens. Matter **18**, 6883 (2006).
[34] E. Plum, J. Zhou, J. Dong, V. A. Fedotov, Th. Koschny, C. M. Soukoulis, and N. I. Zheludev, Phys. Rev. B **79**, 035407 (2009).
[35] J. Zhou, J. Dong, B. Wang, Th. Koschny, M. Kafesaki, and C. M. Soukoulis, Phys. Rev. B **79**, 121104(R) (2009).
[36] S. Zhang, Y. S. Park, J. Li, X. Lu, W. Zhang, and X. Zhang, Phys. Rev. Lett. **102**, 023901 (2009).
[37] M. C. K. Wiltshire, J. B. Pendry, and J. V. Hajnal, J. Phys. Condens. Matter **21**, 292201 (2009).
[38] B. Wang, J. Zhou, Th. Koschny, and C. M. Soukoulis, Appl. Phys. Lett. **94**, 151112 (2009).
[39] X. Xiong, W. H. Sun, Y. J. Bao, M. Wang, R. W. Peng, C. Sun, X. Lu, J. Shao, Z. F. Li, and N. B. Ming, Phys. Rev. B **81**, 075119 (2010).
[40] Z. Li, R. Zhao, Th. Koschny, M. Kafesaki, K. Boratay Alici, E. Colak, H. Caglayan, E. Ozbay, and C. M. Soukoulis, Appl. Phys. Lett. **97**, 081901 (2010).
[41] C. Wu, H. Li, Z. Wei, X. Yu, and C. T. Chan, Phys. Rev. Lett. **105**, 247401 (2010).
[42] R. Zhao, L. Zhang, J. Zhou, Th. Koschny, and C. M. Soukoulis, Phys. Rev. B **83**, 035105 (2011).
[43] Z. Wu, J. Zhu, M. Jia, H. Lu, and B. Zeng, Microw. Opt. Tech. Lett. **53**, 163 (2011).
[44] T. G. Mackay and A. Lakhtakia, SPIE Rev. **1**, 018003 (2010).
[45] A. Andryieuski, C. Menzel, C. Rockstuhl, R. Malureanu, F. Lederer, and A. Lavrinenko, Phys. Rev. B **82**, 235107 (2010).
[46] M. Decker, M. W. Klein, M. Wegener, and S. Linden, Opt. Lett. **32**, 856 (2007).
[47] N. Stefanou, V. Yannopapas, and A. Modinos, Comput. Phys. Commun. **113**, 49 (1998).
[48] N. Stefanou, V. Yannopapas, and A. Modinos, Comput. Phys. Commun. **132**, 189 (2000).
[49] G. Gantzounis and N. Stefanou, Phys. Rev. B **73**, 035115 (2006).
[50] T. Inui, Y. Tanabe, and Y. Onodera, *Group Theory and Its Applications in Physics* (Springer, Berlin, 1990).
[51] M. I. Mishchenko, L. D. Travis, and A. A. Lacis, *Scattering, Absorption, and Emission of Light by Small Particles* (Cambridge University Press, Cambridge, UK, 2002).
[52] N. W. Ashcroft and N. D. Mermin, *Solid State Physics* (Saunders, New York, 1976).
[53] C. Tserkezis, N. Papanikolaou, E. Almpanis, and N. Stefanou, Phys. Rev. B **80**, 125124 (2009).
[54] P. B. Johnson and R. W. Christy, Phys. Rev. B **6**, 4370 (1972).
[55] See Supplemental Material at http://link.aps.org/supplemental/10.1103/PhysRevB.84.125109 for the development of the optical activity characteristics when increasing the number of unit cells along the z direction.